Digital pulse-shape analysis with a TRACE early silicon prototype

D. Mengoni [a,b,*], J.A. Dueñas [c], M. Assié [d], C. Boiano [e], P.R. John [a,b], R.J. Aliaga [f], D. Beaumel [d], S. Capra [e], A. Gadea [g], V. Gonzáles [h], A. Gottardo [i], L. Grassi [a,b], V. Herrero-Bosch [f], T. Houdy [j], I. Martel [c], V.V. Parkar [k], R. Perez-Vidal [g], A. Pullia [e], E. Sanchis [h], A. Triossi [i], J.J. Valiente Dobón [i]

[a] *Dipartimento di Fisica e Astronomia, Università di Padova, via F. Marzolo, 8 - 35131 Padova, Italy*
[b] *INFN Padova, via Marzolo 8 - 35131 Padova, Italy*
[c] *Departamento de Física Aplicada, FCCEE Universidad de Huelva, 21071 Huelva, Spain*
[d] *Institut de Physique Nucléaire, Université Paris-Sud-11-CNRS/IN2P3, 91406 Orsay, France*
[e] *INFN Milano, Via Celoria, 16 - 20133 Milano, Italy*
[f] *Universidad Politécnica de Valencia, CSIC, CIEMAT, I3M, Valencia, Spain*
[g] *Instituto de Fisica Corpuscular, CSIC – Universitat de Valencia, Paterna, Valencia, Spain*
[h] *Departamento de Ingeniería Electrónica, Universitat de Valencia, Burjassot, Valencia, Spain*
[i] *Istituto Nazionale di Fisica Nucleare, Laboratori Nazionali di Legnaro, Legnaro (Padova), Italy*
[j] *Faculté des Sciences, Université Paris-Sud, 91405 Orsay, France*
[k] *Nuclear Physics Division, Bhabha Atomic Research Centre, Trombay, Mumbai 400 085, India*

ARTICLE INFO

Article history:
Received 24 February 2014
Received in revised form
15 July 2014
Accepted 25 July 2014
Available online 10 August 2014

Keywords:
Silicon detector
Light-charged particles
Digital pulse shape analysis
Particle identification
Gamma-ray spectroscopy

ABSTRACT

A highly segmented silicon-pad detector prototype has been tested to explore the performance of the digital pulse shape analysis in the discrimination of the particles reaching the silicon detector. For the first time a 200 μm thin silicon detector, grown using an ordinary floating zone technique, has been shown to exhibit a level discrimination thanks to the fine segmentation. Light-charged particles down to few MeV have been separated, including their punch-through. A coaxial HPGe detector in time coincidence has further confirmed the quality of the particle discrimination.

1. Introduction

The progress in experimental nuclear physics is boosted by the development of new accelerator facilities but also by increasingly sophisticated instruments and techniques for the study of very exotic reaction channels in environment with large background. As a common effort to build up state-of-the-art silicon array for the new experimental setup, the GASPARD-HYDE-TRACE (GHT) [1–3] collaboration has been investigating the limit of detector thickness and sampling frequency for the particle identification by using the digital pulse shape analysis (DPSA).

Whilst highly segmented neutron-transmutated silicon detectors have been proven to achieve an ultimate separation for particles and ions using digital pulse shape analysis [4–7], the question remains to which extent an ordinary floating-zone technique (FZ) detector can be used for the same purpose. Or, in other terms, if the segmentation could provide sufficient homogeneity, which is known to strongly affect the quality of DPSA, in the substrate [8].

The detector thickness is also a long-standing disputed argument to attain the pulse-shape analysis in this context. Augmenting the thickness, whilst making a longer rising time available, elevates the threshold to punch through the first layer and profit of the more robust $\Delta E-E$ technique for particle discrimination.

The type and number of observables determine the number of channel to read out at the preamplifier. Nowadays a very reliable system consists in taking both charge and current signals directly at the preamplifier output [4]. With respect to the aforementioned aspects, in this study we rely on a 200 μm thin FZ silicon detector, with a $4\times4\,mm^2$ segmentation to prove that the DPSA can adequately work by extracting the needed information only from

* Corresponding author at: Dipartimento di Fisica e Astronomia, Università di Padova, via F. Marzolo, 8 - 35131 Padova, Italy.
E-mail address: daniele.mengoni@pd.infn.it (D. Mengoni).

the charge signal. Different approaches are hereby used to discriminate the particles, including the extracted energy *versus* either the maximum of the charge derivative or the rising time.

Such R&D study will pave the way for the development of the new TRacking Array for light Charged particle Ejectiles (TRACE), designed for fusion–evaporation and direct nuclear reactions, which will represent a resident instrument at the Legnaro National Laboratories for the advent of the SPES facility [9].

TRACE is designed to work in tight combination with a gamma array and it was already combined with the AGATA demonstrator [10] to discriminate the reaction channel and provide information for the Doppler correction of the gamma-ray energy [11].

In this paper a single-layer detector, that represents a early TRACE prototype, is combined with a coaxial HPGe detector, previously included in the GASP array [12], to anticipate the experimental setup foreseen for direct reaction at the new generation radioactive beam facilities, such as SPES, SPIRAL2 and HIE-ISOLDE [9,13,14].

2. Experimental setup

The experiment was performed in November 2012 at the Legnaro National Laboratory, Italy. The ^{16}O beam, at 100 MeV, was impinging on a composite target, that comprised a stack of C (80 μg/cm^2), SiO_2 (150 μg/cm^2) and LiF (300 μg/cm^2). The current was on the average 8 enA and the overall rate was below 50 Hz, both for the silicon and the HPGe detector.

The TRACE prototype was placed at approximately 70°, see bottom right corner in the Fig. 1, shown in rectangle. Two other NTD detectors were placed symmetrically relative to the beam axis. Outside the experimental chamber one coaxial HPGe detectors (∼80% intrinsic efficiency), without anti-compton shield, was placed at about 90°, pointing towards the target position. The TRACE highly segmented silicon prototype, wire bounded to the ceramic PCB, is shown in Fig. 2, left. The GASP-type detectors prepared for the experiment are visible in the Fig. 2, right.

From now onward we concentrate only on the TRACE detector. The detector has been produced at FBK-IRST, starting from a n-doped silicon substrate, grown by using a FZ technique. The silicon detector has an active area of 50×20 mm^2 divided in 60 square segments (12 by 5 pads). However, due to the limited number of available electronics channels, only one central pad and the neighboring ones, together with the common electrode, were recorded. The pitch of each segment is 4 mm. The leakage current at 15 V is about 3 nA.

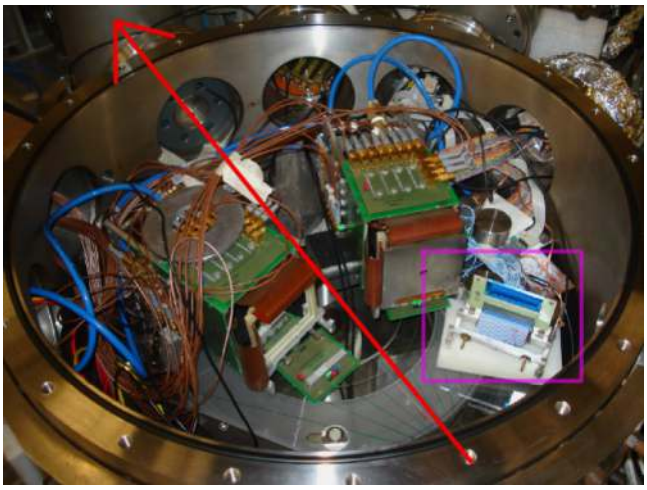

Fig. 1. The experimental setup with the reaction chamber accommodating the three silicon detectors. The TRACE detector, purple rectangle, can be see on the right, with the ohmic side facing the incoming particles. The central pad, only visible on the junction side, is approximately at 70° with respect to the beam direction, sketched in red. (For interpretation of the references to color in this figure caption, the reader is referred to the web version of this article.)

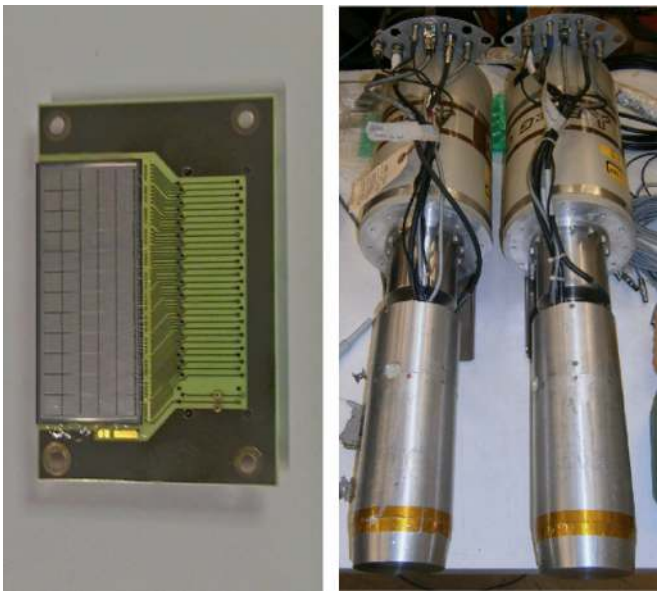

Fig. 2. On the left, the highly segmented silicon-pad detector, used as an early TRACE prototype. The detector is glued and wire bounded onto a ceramic PCB. A total of 60 pads, with a 4-mm pitch, is visible on the junction side, whilst a common electrode is hidden on the ohmic side. The detector has been produced at FBK-IRST. On the right, two GASP coaxial HPGe detectors, of about ∼80% intrinsic efficiency at 1332.5 keV.

Inside the scattering chamber the silicon detector has been connected with a short cable to a 16-channel charge-sensitive preamplifier, designed at INFN Milano [15]. The evaluated equivalent noise charge (ENC) is $(3.3 \pm 0.016/\text{pF})$keV FWHM.

The bandwidth (BW) of 100 MHz guaranteed rising time of less than 5 ns, at 0 pF, and reduced of 0.045 ns per pF of applied capacitance. The preamplifier gain was 45 mV/MeV and the dynamics approximately 100 MeV.

The detector was positioned with the ohmic side facing the particles to enhance the PSA capability. Signals were read and digitized on both sides. The digitization was operated by a 4-channel 100-MHz 14-bit commercial sampling module, CAEN N1728A, with a 2 V input dynamics. The germanium signal was also collected in the same card, which guarantees the synchronization.

The trigger of the acquisition, obtained from a digital leading-edge discriminator embedded in the module, was the central pad of the silicon detector. The rest was only acquired if that signal was present. The signal had a 5 μs baseline before the trigger started. The acquisition windows was 10 μs long.

The acquired signals were afterwards processed to extract the relevant observables, as discussed in the following section.

3. Pulse shape analysis algorithm

The digital signal processing, undergone by the charge output of the silicon-detector preamplifier, is shown in Fig. 3. The analog charge signal is digitized at 100 MHz and its baseline, averaged over 100 points (1 μs), subtracted from the signal. A threshold discriminator is applied to trigger the signals above 10 mV, just above the noise. The signal is processed into two different ways: the one by using a trapezoidal shaping algorithm to obtain the encoded energy information (Q_{max}), and the other by applying an

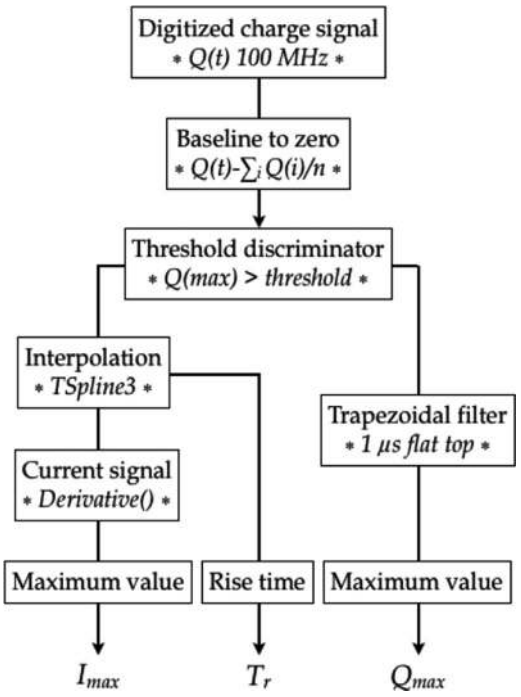

Fig. 3. Flow diagram of the digital signal processing. Three outputs are obtained from the digitized charge signal: energy information encoded in Q_{max}, the rising time of the charge signal T_r, and the peak value of the analytically obtained current signal I_{max}.

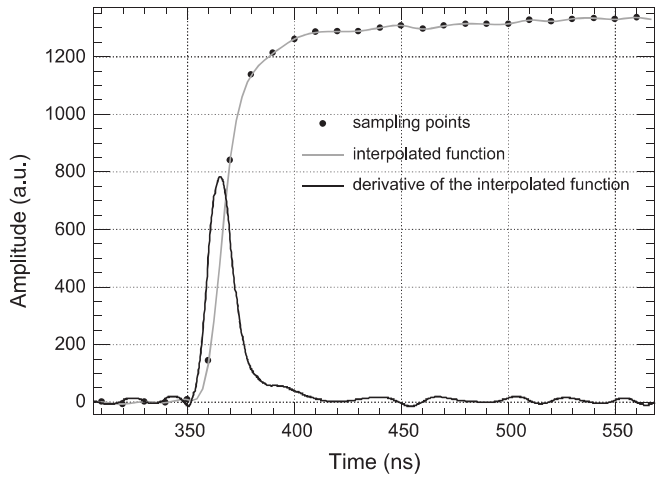

Fig. 4. Digital processing of the charge signal at the preamplifier output. The solid circles represent the sampled points of the charge signal, the light-gray line is the interpolating function and the dark-gray line is the derivative of the interpolating function.

interpolation algorithm to analytically obtain the current signal. The energy, obtained by applying the trapezoidal shaping to the detector pulses, has been calibrated by using the ^{241}Am α-emitter source. The interpolation algorithm is performed using the ROOT class TSpline3 [16], which ensures the first derivative C^1 (slopes match where the curves join) and second C^2 (curvatures match at the join) continuity. Fig. 4 shows the interpolated function (continuos curve) that passes through each of the charge sampling values (filled circles). From the interpolated function the rising time can be obtained with any selected precision since the interpolation can be evaluated at any given time, it was found that good compromise between computing time and precision is achieved for precision values between 10 and 100 ps. The rising time (T_r) was calculated for two given percentages (e.g. 90–10% or 70–30%) of the charge signal maximum, which was obtained by averaging the twenty greatest values. To analytically obtain the current signal we use a derivative function, that is a member of the class TSpline3 mentioned above. This returns the first derivative of the charge interpolated function at point "*x*", see Fig. 4. A stable maximum is found for 50 interpolated points, i.e. above this number of interpolated points the I_{max} reaches a plateau. Correlations between Q_{max} *vs* T_r and Q_{max} *vs* I_{max} are presented in the result section.

4. Correlation with a HPGe detector

A HPGe detector in time coincidence with the particle detector has been placed in the detection setup, to have an independent control over the DPSA on the silicon detector. A malfunctioning preamplifier made eventually only one detector working during the measurement. The charge signal was acquired via an ORTEC preamplifier and sent to the digitizer, as well as the silicon detector. The acquisition trigger, a leading edge discriminator, was set on a pad in the silicon detector, located in the centre of the detector, and the trigger was chosen to be at 5 μs of the 10 μs-long acquisition window. The rest of the channels, including the signal coming from the germanium detector, was acquired in common OR with the silicon detector.

A trapezoidal filter was used to extract the energy observable, by using 2 μs peaking time, equivalent to less than 1 μs shaping time in typical spectroscopic amplifier, and 200 samples for the baseline calculation, and a numerical algorithm, using the maximum of the signal derivative, was chosen to reconstruct *a posteriori* the trigger time for the HPGe detector.

The energy resolution of the HPGe was 3.9 keV at the 1332 keV peak of a ^{60}Co source and the time resolution obtained was about 140 ns.

The gamma rays emitted by the nuclei have to be generally corrected for the velocity of the nucleus and the emission angle. However, being the velocity of emitting nucleus of the order of 0.03 of the speed of light and the detector displaced at about 90°, no Doppler correction has been undertaken. The resulting spectrum is shown in Fig. 5. A prominent line at 511 keV is visible, together with possible neutron contaminations at 608 and 847 keV.

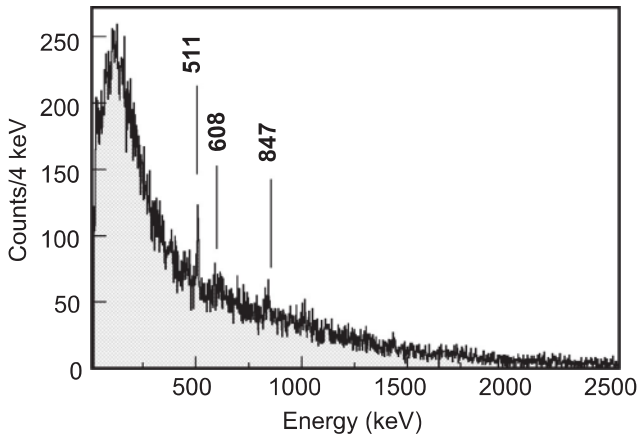

Fig. 5. Gamma-ray energy spectrum. The spectrum is without any applied timing condition and presents the typical 511-keV line in random coincidence with the particle detected in the silicon. Two other broad peaks are visible and possibly due to neutron scattering in the germanium bulk or material surrounding the target.

5. Results and discussion

Various reaction channels were opened by the oxygen beam, with energy much higher than the Coulomb barrier, impinging on the composite target. Direct and compound-nucleus reactions are hereby considered.

Elastic and quasi-elastic processes imply the presence of heavier beam-like or target-like recoils, out of the ADC dynamics. In case of transfer or breakup processes the light particles can be emitted in the angular range covered by the detector, although we expect a forward-focused kinematics for the reaction products. Fusion–evaporation reactions, with the formation of a compound nucleus and the evaporation of light particles, are also included in the possible reaction mechanisms, despite unfavored by the high energy of the beam. A low particle-detection multiplicity is expected in this case due to the small angular coverage of the pad, 4×4 mm^2 large, at variance with emitted particle multiplicity per event, that can reaches values up to 3, see for example Ref. [19].

DPSA was performed on those events that generated the same energy on both the P- and N-side, by the selection of the diagonal line on the energy correlation matrix, that is shown in Fig. 6. The energy *vs* rising time (70–30%) correlation is presented in Fig. 7-top, where it can be clearly seen the ^{1,2,3}H and He curves, and, though with minor statistics, the Li curve. Saturation is reached at about 18 MeV. A noticeable spread in rising time appears at energies close to the punch-through, for each particle, which implies that the signal rising time is very fast in comparison with the sampling rate. This is due to a deficit in sampling points (100 MSPS) that introduces uncertainties on the interpolation and therefore on the rising time calculation, see [17]. As a counter check, in the previous experiment performed by the GHT collaboration, where a sampling rate of 1 GSPS was used, such effect did not manifest [18].

Fig. 7-bottom shows the energy *vs* the mathematically extracted I_{max} correlation. ^{1,2,3}H discrimination is achieved although not as good as the rising time correlation. The broadening effect of the I_{max} with energy is just the result of the previously explained effect of the sampling, which is now transferred mathematically to the I_{max}.

Another locus weakly appears in Fig. 7, which, by extrapolating from the isotopic chain, is likely to be ^{3}He. If it were confirmed, such particle would be here for the first time disentangle from the ^{4}He, by means of DPSA. Typically such particle is not produced in a fusion–evaporation reaction, thus we presume that an other direct reaction mechanism takes place, like the breakup of the Li nuclei, to explain its presence in the correlation plot in Fig. 7.

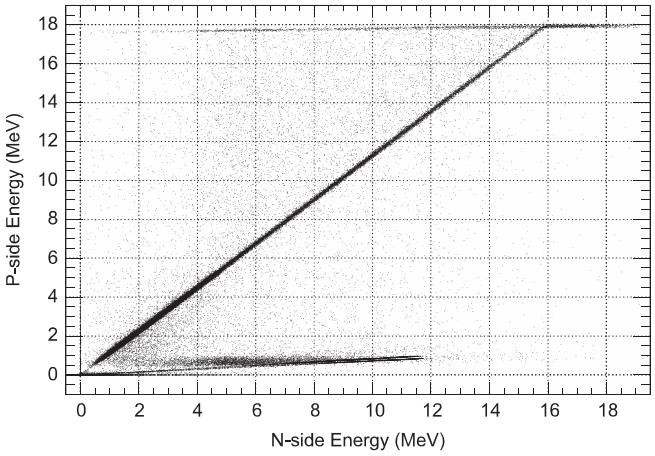

Fig. 6. Energy correlation between P-side and N-side. Analysis was performed on events with P-to-N-side energy ratio of 1.2 (diagonal line).

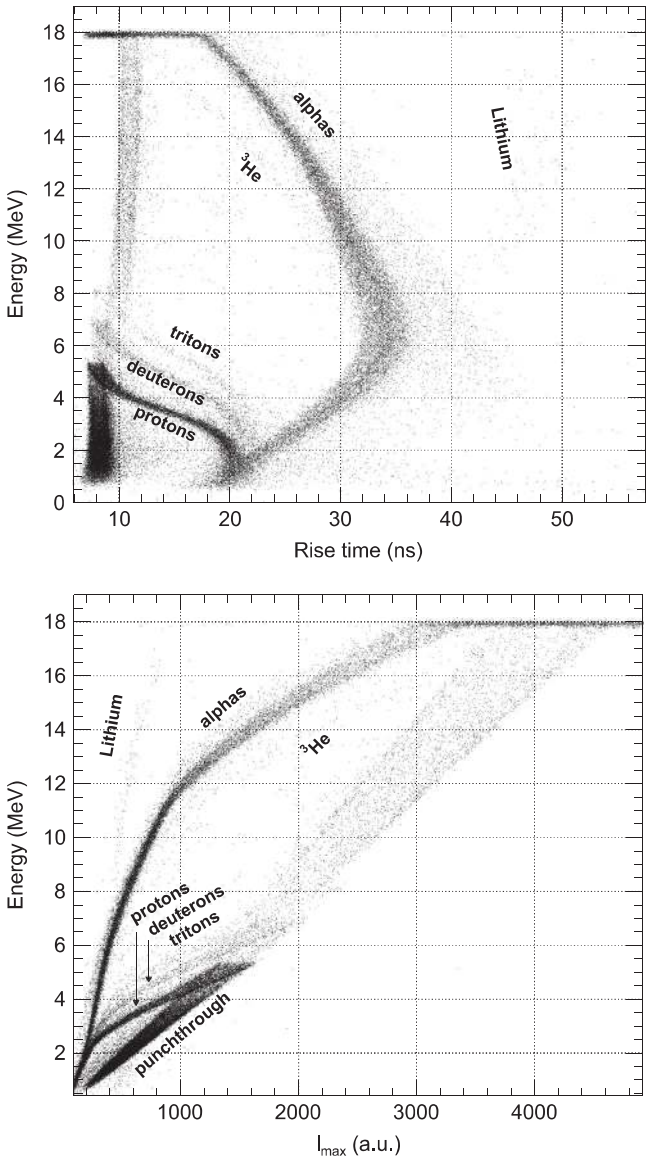

Fig. 7. Top, energy correlation between P-side and N-side. Analysis was performed on events with P-to-N-side energy ratio of 1.2 (diagonal line). Middle, P-side energy *vs* rising time (70 − 30%) correlation. The isotope curves are identify by their corresponding labels.

We quantitatively evaluate the discrimination capability between different isotopes by applying a figure of merit (FoM), according with the definition in Ref [5]. In the present case, we apply an energy cut to the matrix presented in Fig. 7-top. The chosen cut is centred around 4 MeV and is large 40 keV, $\pm$ 20 keV. We obtain a FoM between deutons and tritons of 0.83, above the acceptance threshold (larger than 0.75), see Fig. 8. A better FoM clearly larger than one is obtained between protons and deutons, which means that there is no overlap between the two peaks.

In the gamma-ray energy spectrum, Fig. 5, only the 511-keV peak is evident, if no time gate is applied. When such gate is applied, Fig. 9-top panel, all the visible peaks are in time coincidence with the reaction, following the beam on target. Both such spectra are packed by using a 4 keV/channel bin.

However, this does not guarantee that such peaks are emitted from nuclei directly populated in the reactions as they could be originated by the neutrons elastically scattered either in the bulk of the HPGe detector or in the surrounding materials. These transitions are commonly concentrated around 600 keV and 800 keV, and

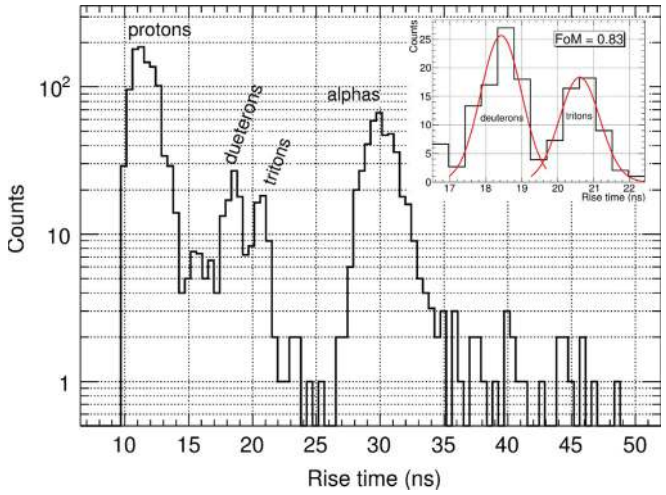

Fig. 8. Projection of the correlation matrix in Fig. 7-top, when an energy cut, centred at 4 MeV and large 40 keV, ± 20 keV, is applied. In the inset the separation between the two most neighboring peaks is estimated by using a figure of merit (FoM), see text for details. The result gives a value which is above our acceptance threshold, larger than 0.75.

show a typical triangular shape, for the de-excitation of naturally abundant ^{70,72,74,76}Ge isotopes in the bulk of the detector. Alternatively, the mechanical structure, such as the beam pipe, the reaction chamber or the beam stopper could also act as a neutron scatterer and emit gamma rays, which would result in time coincidence with the particle detection and therefore with the beam reactions. These peaks are typically from Al (844-, 1014- and 2211-keV lines), Fe (847-keV line) and Pb (2615-keV line). For a detailed description see for example Ref. [20] and references therein. In principle the neutron–gamma discrimination can be successfully achieved if the time resolution of the detectors is good enough and if the variation in the flight time, due to the finite detector thickness, is small enough for the neutron energy range of interest. However, even the narrowest time gate cannot usually prevent from seeing the contamination by fast neutrons, up to 10 MeV, interacting with the material near the target position.

In our case the time gate is 140 ns, which is long enough for low-energy neutrons to reach the germanium detector, approximately 20 cm away from the target position. Indeed, in the spectrum a gamma line at 847 keV is evident, preceded at about 608 keV by a bump which has the typical shape produced by the neutron scattering on germanium detector. Therefore, we conclude that the 847-keV line is either from ^{56}Fe or from ^{76}Ge, excited by higher-energy neutrons.

Two bi-dimensional conditions, for protons and α particles, have been obtained from the matrix in Fig. 7, bottom panel. When the particle conditions are alternatively applied, in addition to the time gate, the gamma-ray spectra, in the middle and bottom panel of Fig. 9, are obtained for protons and alpha particles respectively. Some peaks weakly start to appear at energies higher than 1 MeV, where the neutron contamination is less important, predominantly in the proton channel. Excluding the even–even light nuclei, whose excitation energy of the low-lying states is too high to be detected with sufficient statistics, few odd–even nuclei remain, having mass number between 20 and 36, as possible candidates for the emission of these gamma rays. We assign all these transitions to ^{36}Cl, populated in the ^{28}Si(^{16}O,α 3p1n)^{36}Cl channel, except the 1567-keV transition, which is assigned to ^{21}Ne, populated by the ^{12}C (^{16}O,1α 2p1n)^{21}Ne reaction. In the case of the α-channel spectrum, Fig. 9-bottom panel, the poor statistics impedes from firmly identify any peaks, especially at energies above 1 MeV. Nevertheless we

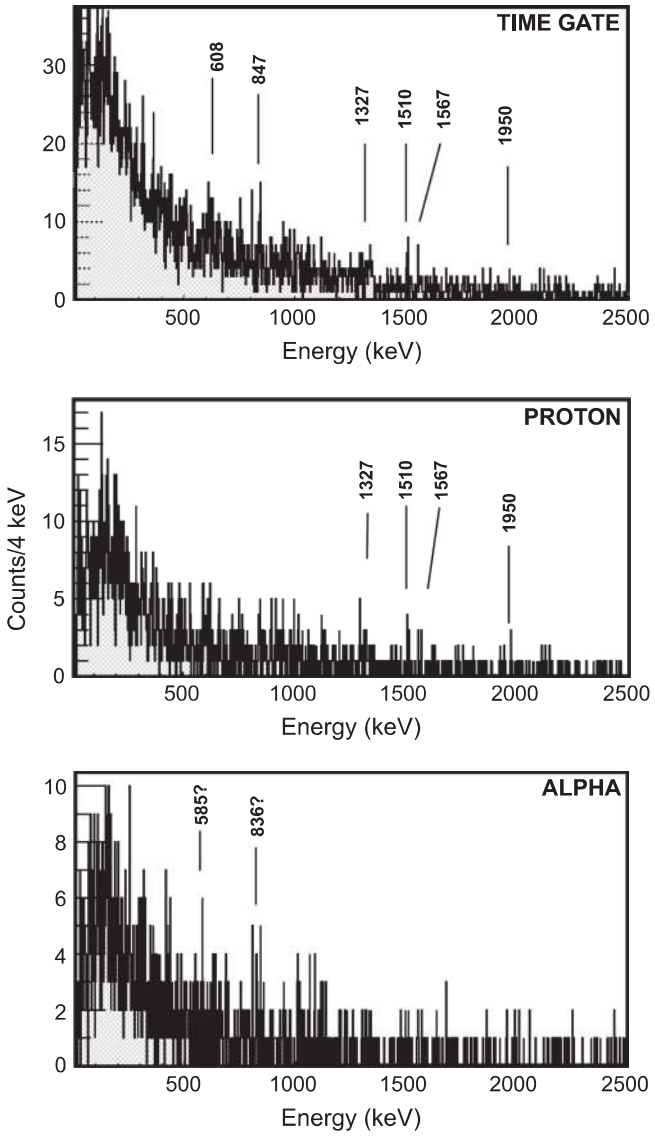

Fig. 9. Gamma-ray energy spectra. In the top panel, the spectrum obtained by applying a time gate is applied. In the middle and bottom panel, a spectrum in coincidence with protons and α particles, respectively.

hazard the possible presence of peaks from ^{25}Mg, populated by ^{19}F (^{16}O,2α 1p1n)^{25}Mg.

It is not possible in principle to assign unequivocally the gamma transitions seen in the spectra to a unique reaction channels as most of them involve both α-particle and proton emission. However it as to be noted that the gamma lines are in coincidence with those nuclei that are produced in the reaction channels with the higher number of particles emitted, which is a further confirmation of the correct interpretation of the DPSA results, obtained by using the silicon detector.

6. Summary and conclusions

In this paper we investigated the quality of the digital pulse shape analysis obtained by using a segmented 200 μm thin silicon detector, obtained with a FZ growing technique. In the experiment the TRACE highly segmented silicon pad detector was assisted by a coaxial HPGe GASP detector to further prove the outcome of pulse shape analysis.

The digitized charge signal has been processed to obtain the energy, the maximum of the derivative (current signal) and the rising time. The correlation matrix, either energy *vs* the maximum of the current or *vs* rising time, confirms the high quality of the pulse shape analysis that can be safely pursued using this approach, up to the punch-through energy.

Light isotopes, ^{1,2,3}H, can be easily separated among them and between the αparticles. In addition the discrimination of ^{3}He from the ^{4}He is proposed here for the first time. A lower discrimination threshold can be established for proton down to 2 MeV, by using the energy *vs* rising time correlation.

Furthermore, particle discrimination has been searched from gamma-ray transitions in time coincidence with the particle emission. Although the reaction channel could not be unambiguously determined, for the concurrent emission of more than one particles and for the marginal statistics, the resolved gamma rays seem to be populated in the channel with the higher particle multiplicity, as a further confirmation of the quality of the pulse shape analysis coming from the silicon detector.

In conclusion the uniformity of the silicon detector, here guaranteed by the fine pad segmentation, provide a good particle discrimination also for detector layer thin only 200 μm.

In the future we plan to conduct a systematic study of a possible enhancement of the spatial resolution with respect to the geometrical one, when the transient signals of the electrodes, neighboring to the one collecting the net charge, are considered. Furthermore, a full characterization of the integral and differential cross-talk signals, aiming at their correction, is also planned. A laser scan of the bulk uniformity is also envisaged.

Acknowledgments

This work has been supported by the Italian Ministry of Education, University and Research (MIUR) under the project FIRB/08-RBFR08RDKZ and partially supported by the Spanish Ministry of Science and Innovation (MICINN) under projects FPA2007-63074 (FINURA) and INGENIO-2010 (CPAN). The research leading to these results has received funding from the European Union Seventh Framework Programme FP7/2007–2013 under Grant Agreement no. 262010 – ENSAR. One of the authors (V.V. P.) acknowledges the financial support through the INSPIRE faculty program, Department of Science and Technology, Government of India, in carrying out these investigations. The authors would like to extend appreciation to the technical staff of LNL Tandem for their assistance during the experiment and the local members of the EXOTIC project for their support in the preparation of the experimental setup.

References

[1] D. Beaumel, Nuclear Instruments and Methods in Physics Research Section B 317 (2013) 661.
[2] I. Martel, et al., in: Proceedings of the DAE Symposium on Nuclear Physics, vol. 55, 2010, p. I12.
[3] A. Gadea, et al., Nuclear Instruments and Methods in Physics Research Section A 654 (2011) 88.
[4] J.A. Duenas, et al., Nuclear Instruments and Methods in Physics Research Section A 676 (2012) 70.
[5] J.A. Duenas, et al., Nuclear Instruments and Methods in Physics Research Section A 714 (2013) 48.
[6] B. Genolini, Nuclear Instruments and Methods in Physics Research Section A 732 (2013) 87.
[7] L. Bardelli, et al., Nuclear Physics A 654 (2011) 272.
[8] F.Z. Henari, et al., Nuclear Instrument and Methods A 288 (1990) 439.
[9] ⟨https://web.infn.it/spes/index.php/characteristics/documents/tdr-2012⟩.
[10] S. Akkoyun, et al., Nuclear Instruments and Methods A 668 (2012) 26.
[11] F.C.L. Crespi, EPJ Web of Conference, in: Proceeding at the INPC, 2–7 June 2013, Florence.
[12] D. Bazzacco, et al., in: Proceedings of International Conference in Nuclear Structure at High Angular Momentum, Ottawa, p. 376, 1992. AECL-10613 (1992).
[13] ⟨http://pro.ganil-spiral2.eu/spiral2⟩.
[14] ⟨http://hie-isolde.web.cern.ch/hie-isolde/⟩.
[15] E. Strano, et al., Nuclear Instruments and Methods B 317 (2013) 657.
[16] ROOT – An Object Oriented Data Analysis Framework, ⟨http://root.cern.ch/root/html/TSpline3.html⟩.
[17] L. Bardelli, et al., Nuclear Instrument and Methods A 521 (2004) 480.
[18] J.A. Dueñas, et al., Nuclear Instrument and Methods A 743 (2014) 44.
[19] E. Farnea, et al., Nuclear Instrument and Methods A 400 (1997) 87.
[20] M. Şenyiğit, et al., Nuclear Instruments and Methods in Physics Research Section A 735 (2014) 267.